Synthesis of Y_2O_3 Nanocrystals and the Effect of Nanocrystalline Y_2O_3 Supports on Ni/Y_2O_3 Catalysts for Oxidative Steam Reforming of Ethanol

Gebiao Sun, Kus Hidajat, and Sibudjing Kawi*
Department of Chemical and Biomolecular Engineering, National University of Singapore, 4 Engineering Drive 4, 119260, Singapore

(Received August 14, 2006; CL-060930; E-mail: chekawis@nus.edu.sg)

Y_2O_3 nanocrystals of tunable morphology and size have been successfully synthesized; the mobility of surface oxygen species on Y_2O_3 nanocrystals is found, for the first time, to increase with the decrease of the crystal size and to significantly affect the catalytic performances of Ni/Y_2O_3 catalysts for oxidative steam reforming of ethanol.

The shortage of energy sources and environmental problems have prompted intense research interest in hydrogen production, purification, storage, and utilization.[1–4] Alcohol reforming is considered to be a competitive route for hydrogen production because of its mild requirements for reforming conditions.[5,6] Since nickel is found to be an active metal for oxidative steam reforming of ethanol,[6] many oxides have been investigated as the support of nickel metal catalyst in order to obtain a catalyst of high performance for efficiently producing hydrogen from this reaction system. It has been reported that nickel supported on some oxides, such as Y_2O_3, exhibits much better catalytic performance than that supported on other oxides such as Al_2O_3.[7] However, up to now, it is still not clear yet how Y_2O_3 support promotes the nickel-catalyzed oxidative reforming reaction of alcohol.

In the present study, four Y_2O_3 supports with different morphologies and crystal sizes have been successfully synthesized and investigated as the supports of Ni-based catalysts for oxidative steam reforming of ethanol. The influence of Y_2O_3 crystal size on the catalytic performance of Ni/Y_2O_3 has also been investigated in order to obtain a fundamental understanding on the role of nanocrystalline support in oxidative reforming reaction.

Y_2O_3 samples with systematically varied crystal sizes were synthesized under different pH-controlled hydrothermal conditions. A typical synthesis of Y_2O_3 is as follows: 7.66 g of $Y(NO_3)_3 \cdot 6H_2O$ was dissolved in 100 mL of deionized (DI) water. $NH_3 \cdot H_2O$ was added to the yttrium nitrate solution to control the solution pH at 7, 9, 11, or 12. The resultant slurry was transferred to an autoclave and hydrothermally treated at 170 °C for 20 h. The solid material was recovered, washed, and fully dried. Finally, crystalline Y_2O_3 was obtained after calcination in air at 800 °C for 5 h. These four Y_2O_3 samples synthesized at pH 7, 9, 11, and 12 are designated as Y7, Y9, Y11, and Y12, respectively.

Ni/Y_2O_3 catalysts were prepared by wet impregnation. Typically, 1.4 g of Y_2O_3 (either Y7, Y9, Y11, or Y12) and 0.3 g of $Ni(NO_3)_2 \cdot 6H_2O$ were added to 40 mL of DI water under vigorous stirring followed by drying and calcination in air at 600 °C for 5 h. The Ni contents of the resultant four catalysts (Ni/Y7, Ni/Y9, Ni/Y11, and Ni/Y12), as analyzed by ICP, were all around 3.7 wt %. For each test, 100 mg of catalyst was used, which was reduced under hydrogen at 450 °C for 30 min prior to the catalytic test.

Figure 1 clearly indicates that the synthesis pH affects the morphology of Y_2O_3. Y7 has a sheet-like shape with thickness of ≈200 nm. Y9 has hexagonal prism morphology with diameter of ≈2 μm and length of several micrometers. Y11 has nanorod-like structure with diameter of ≈100 nm. Y12 has nanosheet-like shape with much thinner thickness of only ≈10 nm. Although the synthesis of Y_2O_3 prism, nanorods, nanotubes or mesostructured Y_2O_3 has been reported elsewhere,[8] to our knowledge, this is the first report of the synthesis of uniform and stable Y_2O_3 nanosheet.

The crystal sizes of these Y_2O_3 samples (calculated by using Debye–Scherrer equation) are found to decrease with increasing synthesis pH. They are ≈38, 25, 19, and 9 nm for Y7, Y9, Y11, and Y12, respectively. Interestingly, the crystalline size of the Y_2O_3 support is found to affect the catalytic performances of Ni/Y_2O_3 catalysts. As shown in Table 1, Ni/Y12 catalyst gives the highest H_2 production rate at the temperature range of 500–750 °C while Ni/Y11, Ni/Y9, and Ni/Y7 catalysts give sequentially descending H_2 production rate, showing that the catalytic performances of Ni/Y_2O_3 catalysts increase with the decrease of crystalline size of Y_2O_3.

In order to reveal how these nanocrystalline Y_2O_3 supports affect the catalytic performance, a series of characterizations have been conducted. Data listed in Table 1 show that the specific surface areas of the catalysts, particle size, and dispersion of nickel on Y_2O_3 do not differ greatly, suggesting that they may not be the key factors in causing the difference of the catalytic performance. In addition, H_2-TPR analysis of Ni/Y_2O_3 catalysts (see Supporting Information)[12] shows that the reducibility of Ni on all these catalysts is not affected by the crystal size of the sup-

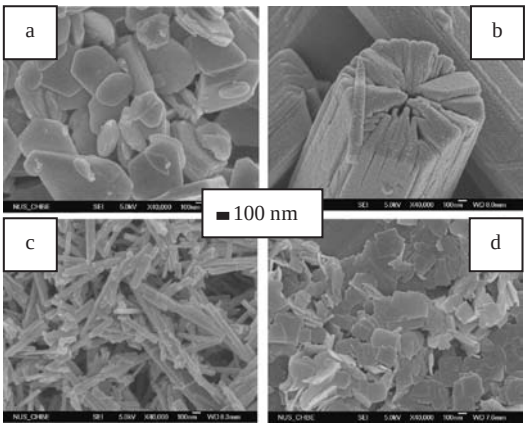

Figure 1. FESEM images of Y_2O_3 synthesized at pH a) 7; b) 9; c) 11; d) 12.

Table 1. Property and performance of Ni/Y_2O_3 catalysts

	S_{BET}	Ni particle size[a]	Ni dispersion[a]	H_2 Production rate $\times 10^{-2}$ ($moleH_2/KgNi/h$)[b]			
	$/m^2\,g^{-1}$	/nm	/%	500 °C	600 °C	700 °C	750 °C
Ni/Y7	30	≈15	12	310.9	441.0	580.8	633.3
Ni/Y9	22	≈13	11	329.5	450.3	620.6	663.9
Ni/Y11	29	≈14	13	362.0	479.0	656.2	678.3
Ni/Y12	46	≈16	13	381.1	499.1	680.1	700.1

[a]Measured from H_2-TPD. [b]Molar ratio of $C_2H_5OH:H_2O:O_2 = 1:3:0.5$; GHSV = $44170\,h^{-1}$; Carrier gas (N_2): 30 mL/min.

port. Furthermore, XPS analysis of Ni/Y_2O_3 catalysts (see Supporting Information)[12] shows that there is no reaction between Ni and Y_2O_3, suggesting that the difference in catalytic performance of these catalysts neither results from the association between Ni and Y_2O_3 support.

The H_2-TPR profiles of the synthesized Y_2O_3 (Figure 2) show that Y_2O_3 can be reduced. However, the low intensity of the reduction peak indicates that Y_2O_3 can only be partially reduced at the temperature range of 500–800 °C. It is believed that the hydrogen molecules can only consume the oxygen located on the surface of Y_2O_3, hence the position and intensity of the H_2 consumption peaks could be used to indicate the surface oxygen mobility of these oxide samples.[9,10] It can be seen from Figure 2 that the maximum height of Y7 appears at ≈700 °C while that of Y12 at ≈600 °C, indicating that the surface oxygen mobility increases from Y7 to Y12 since the lower temperature at which the reduction peak appears, the higher oxidizing ability/oxygen mobility an oxide exhibits.[9] This increase probably results from the decrease of crystal size because the smaller the crystal, the higher the surface energy and hence the more active the surface oxygen species. It is also noted from Figure 2 that the intensities of these peaks sequentially increase in the order of Y7, Y9, Y11, and Y12, suggesting that the available amount of mobile surface oxygen species increases in the same order. The amount of mobile surface oxygen species could be significantly affected by the amount of interstitial oxygen ions because it has been reported[10] that the mobile oxygen in an oxide crystal is provided by the interstitial oxygen ions. It is also believed that the more crystal defects an oxide possesses, the larger amount of interstitial oxygen ions it contains.[10] Therefore, it is very likely that Y12, which has the smallest crystal size, possesses the largest amount of crystal defects and hence the largest amount of mobile oxygen species, while Y7, Y9, or Y11, which has larger crystal size, possesses more perfect crystalline structure with fewer defects and hence smaller amount of mobile surface oxygen species. This observation explains why the amount of mobile surface oxygen species increases with the decrease of crystal size.

It is interesting to note that the order of mobility of surface oxygen species on Y_2O_3 supports is similar with that of the catalytic performance of the corresponding Ni/Y_2O_3 catalyst, suggesting that the surface oxygen mobility of Y_2O_3 support is the key factor in causing the difference in catalytic performance. Although mobile surface oxygen species on a support has been found to play an important role in other catalytic system, such as CO oxidation reaction,[11] this is the first time that the surface oxygen species provided by the support is found experimentally to play a crucial role in the ethanol oxidative steam reforming reaction. Therefore, the difference in catalytic performance of these Ni/Y_2O_3 catalysts associated with the variation of the crystal size of Y_2O_3 supports can be attributed to the difference in the mobility of the surface oxygen on the supports.

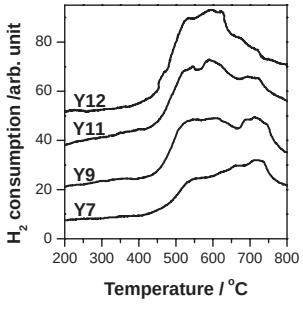

Figure 2. H_2-TPR profiles of crystalline Y_2O_3 supports.

In summary, the morphology and crystal size of Y_2O_3 supports can be controlled using pH-controlled hydrothermal synthesis conditions. The dispersion and particle size of the impregnated nickel species are not affected by the variation of the crystal size of Y_2O_3. However, the change of crystal size of Y_2O_3 supports results in the difference in the mobility of surface oxygen species on Y_2O_3. The surface oxygen mobility has been identified to play a crucial role in influencing the catalytic performance of Ni/Y_2O_3 catalyst on oxidative steam reforming of ethanol.

The authors acknowledge financial support from National University of Singapore (Grant R-151-112).

References and Notes

1 C. S. Song, *Catal. Today* **2006**, *115*, 2.
2 A. Neramittagapong, S. Hoshino, T. Mori, J. Kubo, Y. Morikawa, *Chem. Lett.* **2002**, *31*, 1078; Y. Sekine, S. Asai, K. Urasaki, M. Matsukata, E. Kikuchi, S. Kado, F. Haga, *Chem. Lett.* **2005**, *34*, 658; Y. Xu, Z. Tian, G. Wen, Z. Xu, W. Qu, L. Lin, *Chem. Lett.* **2006**, *35*, 216; J. J. Strohm, J. Zheng, C. S. Song, *J. Catal.* **2006**, *238*, 309.
3 S. Horinouchi, Y. Yamanoi, T. Yonezawa, T. Mouri, H. Nishihara, *Langmuir* **2006**, *22*, 1880.
4 J. Tong, Y. Matsumura, *Appl. Catal., A* **2005**, *286*, 226; J. Tong, L. Su, K. Haraya, H. Suda, *Chem. Commun.* **2006**, 1142; J. Tong, Y. Matsumura, *Catal. Today* **2006**, *111*, 147.
5 G. A. Deluga, J. R. Salge, L. D. Schmidt, X. E. Verykios, *Science* **2004**, *303*, 993; K. Urasaki, K. Tokunaga, Y. Sekine, E. Kikuchi, M. Matsukata, *Chem. Lett.* **2005**, *34*, 668; J. Kugai, V. Subramani, C. S. Song, M. H. Engelhard, Y. H. Chin, *J. Catal.* **2006**, *238*, 430.
6 A. N. Fatsikostas, D. I. Kondarides, X. E. Verykois, *Chem. Commun.* **2001**, 851.
7 J. Sun, X. Qiu, F. Wu, W. Zhu, *Int. J. Hydrogen Energy* **2005**, *30*, 437.
8 X. Wang, X. Sun, D. Yu, B. Zou, Y. Li, *Adv. Mater.* **2003**, *15*, 1442; J. Zhang, Z. Liu, J. Lin, J. Fang, *Cryst. Growth Des.* **2005**, *5*, 1527; J. Guzman, A. Corma, *Chem. Commun.* **2005**, 743.
9 S. S. Lin, C. L. Chen, D. J. Chang, C. C. Chen, *Water Res.* **2002**, *36*, 3009.
10 E. Mamontov, T. Egami, R. Brezny, M. Koranne, S. Tyagi, *J. Phys. Chem. B* **2000**, *104*, 11110.
11 J. Guzman, S. Carrettin, A. Corma, *J. Am. Chem. Soc.* **2005**, *127*, 3286; J. Guzman, S. Carrettin, J. C. F. Gonzalez, Y. Hao, B. C. Gates, A. Corma, *Angew. Chem., Int. Ed.* **2005**, *44*, 4778.
12 Supporting Information is available electronically on the CSJ-Journal website, http://www.csj.jp/journals/chem-lett.

Published on the web (Advance View) October 25, 2006; doi:10.1246/cl.2006.1308